The Enhancing Effect of α–FeOOH on Ni Surfaces Toward Electrolytic Water Splitting

Megan M. Heath, Fatemeh Poureshghi, Frode Seland, Svein Sunde, and Roelof J. Kriek*

For decades Ni has been known as an electrocatalyst for the oxygen evolution reaction (OER); however, the crucial role that Fe plays in enhancing the electrocatalytic activity of Ni still requires deeper investigation and understanding. Herein, some light on the role of Fe by studying the structural evolution of different Ni-based electrocatalysts upon the electrolytic addition of different quantities of Fe are shaded. Colloidal Ni and NiO, as well as Ni, NiO, and NiNiO nanoparticles, are synthesized and electrochemically characterized in Fe-free and Fe-doped KOH electrolytes. Voltammetry and in situ Raman spectroscopy show that higher concentrations of Fe in the electrolyte lead to lower OER overpotentials due to the presence of α–FeOOH.

1. Introduction

Worldwide, the need for clean and renewable energy sources continues to grow. Renewable energy sources, such as wind and solar, are intermittent, and the produced energy needs to be stored. Electrochemical water splitting through alkaline water electrolysis serves as a viable solution to this problem, as it stores energy in the form of hydrogen by splitting water into hydrogen and oxygen. Two half-cell reactions are involved in water splitting: the hydrogen evolution reaction and the oxygen evolution reaction (OER). In alkaline environments, both reactions contribute to the rather large overpotential required and require efficient electrocatalysts to operate at a practical rate. Ni has been proven to be an excellent OER electrocatalyst in alkaline media,[1,2] and a large variety of Ni and Ni-based nanoparticles have been explored as electrocatalyst material in recent years.[3] These nanoparticles often have various morphologies and oxidation states.[4–9] The oxidation states are said to have an impact on the OER performance.[10]

Corrigan found that Fe impurities in the alkaline electrolyte are responsible for the enhanced activity of Ni toward the OER.[11] Since then, many studies of Ni electrocatalysts toward the OER have been carried out in reagent grade KOH. These studies report excellent OER activities for Ni with low overpotentials (around 330 mV at 10 mA cm^{-2}),[12–14] while possibly allowing for electrolytic Fe to influence the OER activity. Years after Corrigan's study,[11] another study on this topic was published, where rigorously purified KOH was used to indicate that Ni has a much lower OER activity without the presence of Fe.[15] In addition, numerous studies have been conducted on cosynthesized NiFe electrocatalysts during the past few decades.[16–20] Although it is known that Fe enhances the OER activity of Ni, it is not clear how this activity increase is attained. In addition, it is still an ongoing debate as to whether Ni or Fe is the OER active site. It is integral from an electrocatalyst design perspective to understand how Ni electrocatalysts are influenced by Fe. An important point of departure is to understand how unintentional Fe (Fe originating from the electrolyte or other impurities) affects the electrochemical activity and structure of Ni electrocatalysts.

Raman spectroscopy is a sensitive technique in the low-frequency range where the characteristic vibrations of metal oxides, hydroxides, and oxyhydroxides appear.[21] Therefore, Raman is a suitable technique to use for the in situ analysis of Ni and Fe OER electrocatalysts and the intermediate and active sites involved.[22,23] In situ Raman spectroscopy has been employed in a previous study to investigate Ni electrocatalysts aged in purified KOH and reagent grade KOH (containing ≤0.66 ppm Fe).[24] It was found that Fe replaced some of the bulk Ni to form a NiFe-layered double hydroxide (LDH).[24]

In this work, in situ Raman spectroscopy, along with voltammetry, was used to investigate the active structures of Ni OER electrocatalysts in Fe-doped KOH. Two different morphologies and different oxidation states of Ni were

M. M. Heath, R. J. Kriek
Electrochemistry for Energy & Environment Group
Research Focus Area: Chemical Resource Beneficiation (CRB)
North-West University
Potchefstroom 2520, South Africa
E-mail: cobus.kriek@nwu.ac.za

F. Poureshghi, F. Seland, S. Sunde
Department of Materials Science and Engineering
Norwegian University of Science and Technology (NTNU)
NO-7491 Trondheim, Norway

The ORCID identification number(s) for the author(s) of this article can be found under https://doi.org/10.1002/ente.202300313.

investigated. It was found that electrolytic Fe enhances the OER activity of the Ni, NiO, and NiNiO electrocatalysts tested and that the increased activity can be ascribed to the presence of α–FeOOH on the surface of these electrocatalysts.

2. Results and Discussion

2.1. Physical Characterization

Figure 1 shows that the colloidal nanoparticles synthesized with the tailored synthesis method have spherical morphology. The spheres are not interconnected, as individual spheres can easily be identified. The average diameter of the colloidal Ni nanoparticles is 17.47 nm and that of the particles prepared by the chemical reduction synthesis method is 21.90 nm. Histograms of the size distribution can be seen in the supporting information. The morphology of these irregular-shaped particles can be described as interconnected curved sheets. These particles will be referred to in this paper simply as nanoparticles.

The diffraction patterns of colloidal NiO nanoparticles (**Figure 2**a) and NiO nanoparticles (Figure 2b) show sharp peaks at 2θ values of 37.2°, 43.2°, and 63.0°. These peaks correspond to the (111), (200), and (220) phases of face-centered cubic (fcc) NiO

Figure 1. TEM images of the synthesized a) colloidal nanoparticles (tailored synthesis) and b) nanoparticles (chemical reduction).

as indexed in PDF Card-00-047-1049 for NiO (bunsenite). In addition, colloidal NiO has a peak at 75.6° that corresponds to the (311) plane of the fcc phase of NiO.[25] The diffraction patterns of colloidal Ni (Figure 2a) and Ni nanoparticles (Figure 2b) show two sharp peaks at 44.6° and 51.8°. Colloidal Ni has an additional peak at 76.5°. These three peaks correspond to the (111), (200), and (220) phases of Nickel, PDF Card-04-010-6148. Lastly, NiNiO nanoparticles have peaks at 37.2°, 44.5°, 51.8°, and 62.8°, indicating that the diffractogram of NiNiO is the diffractograms of Ni and NiO superimposed. The peaks at 22° and 26° arise due to the Kapton film used in the sample preparation for powder XRD. The Rietveld refinements of the diffractograms can be seen in Section 3 of the supporting information. This illustrates that phase-pure samples have been prepared and that the NiNiO sample consists of 63.74% Ni and 36.26% NiO. The crystallite sizes calculated from the Rietveld refinement can be found in Table S1, Supporting Information.

X-ray photoelectron spectroscopy (XPS) analysis was also performed on these electrocatalysts and can be found in Section 4 in the supporting information. XPS provides additional confirmation that the desired samples were successfully prepared. The samples were analyzed after 30 cyclic voltammetry (CV) cycles in each electrolyte composition, and the effect of cycling in Fe-containing electrolytes on the oxidation states can be observed. It was found that Ni is more easily oxidized than NiO, in agreement with what has been reported in the literature.[20] In addition, the trend observed by Nardi et al.,[26] i.e., that increasing the Fe concentration leads to less oxidized films are observed for some of the samples in this study.
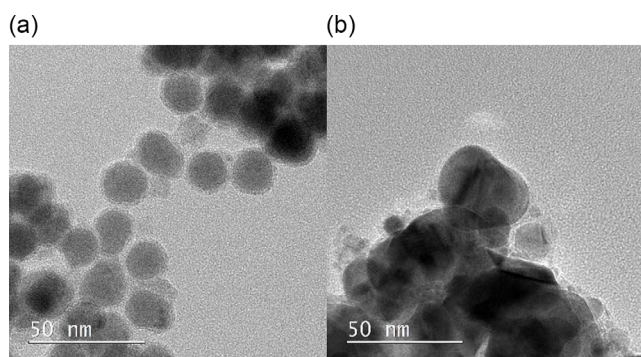
2.1.1. Electrochemistry

Each catalyst sample was cycled 30 times to precondition the electrocatalyst and provide time for Fe incorporation (Figure S10, Supporting Information). **Figure 3** overlays the CVs after 30 preconditioning cycles of each electrocatalyst in each electrolyte composition. This figure shows the relative sizes and positions of each oxidation wave. All catalysts show similar voltammetric features after 30 potential scans (Figure 3), with an oxidation peak at around 1.4 V in the positive-going sweep and a
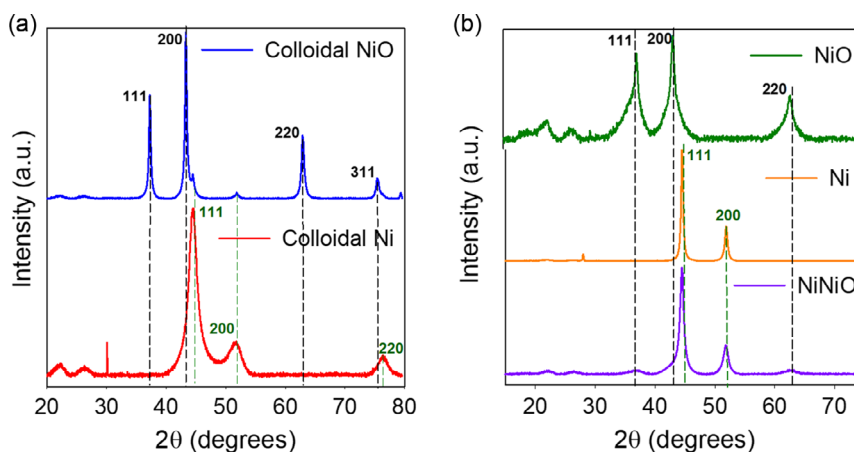

Figure 2. Powder XRD patterns of a) the two colloidal nanoparticles (Ni and NiO) and b) the three nanoparticle electrocatalysts (Ni, NiO, and NiNiO) prepared.
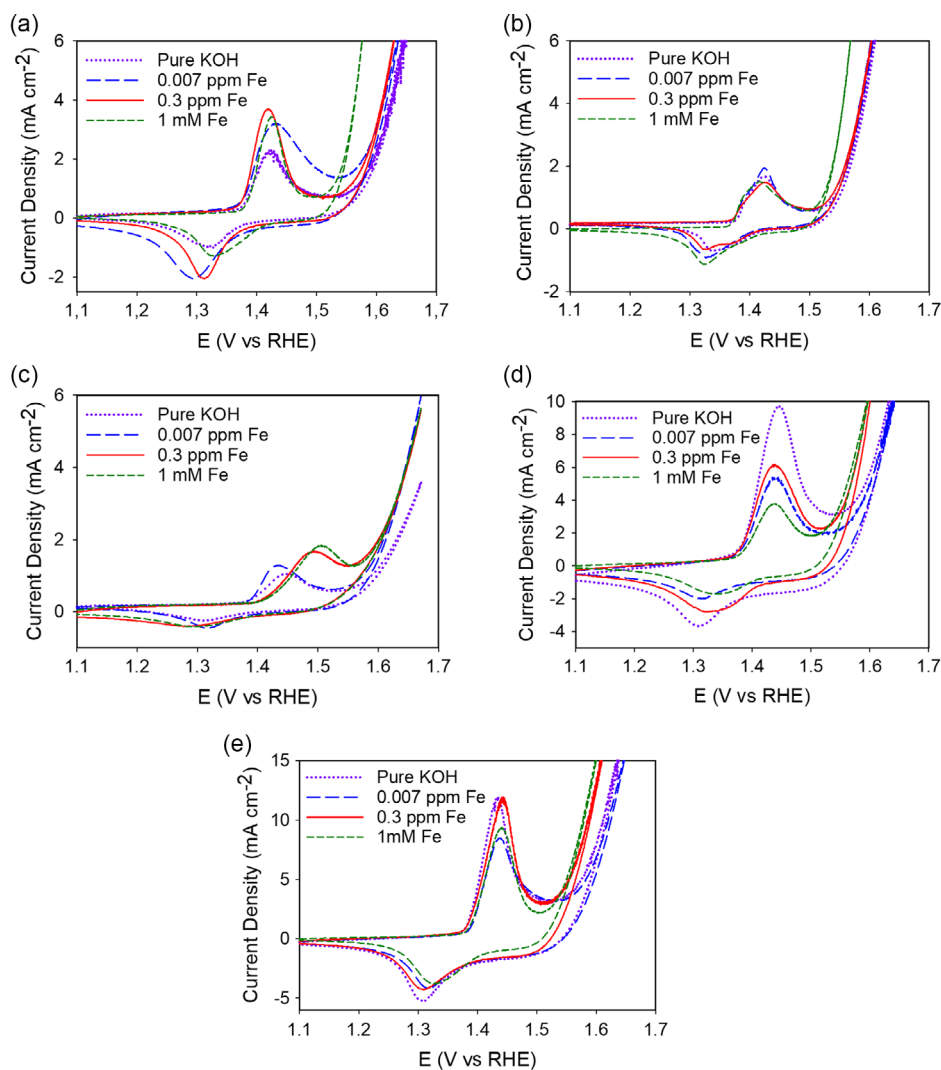
Figure 3. Cyclic voltammograms of a) colloidal Ni, b) colloidal NiO, c) Ni nanoparticles, d) NiO nanoparticles, and e) NiNiO nanoparticles, after cycling 30 times in pure KOH and KOH doped with 0.007 ppm, 0.3 ppm, and 1 mM Fe.

corresponding reduction peak at 1.3 V in the subsequent negative-going sweep. The oxidation peak corresponds to the oxidation of $Ni(OH)_2$ to $NiOOH$, and the reduction peak corresponds to the reduction of $NiOOH$ back to $Ni(OH)_2$.[27,28] It is known that a thin layer of oxide is formed immediately when a Ni electrode comes in contact with air.[27] Furthermore, when immersed in an alkaline solution, a film of $Ni(OH)_2$ is spontaneously formed on the surface of the electrocatalyst.[9,14]

The influence of iron additions on this voltammetric features is small as it relates to the nickel redox transition. However, iron has a large impact on the onset of the OER, observed at potentials above 1.5 V. The position of the oxidation peak does not shift much after cycling the samples in KOH containing different concentrations of Fe. Previous studies report that the oxidation peak shifts to more positive potentials when more Fe is incorporated into the bulk electrocatalyst structure.[15,29] It is also reported that the oxidation peak becomes smaller when increased amounts of Fe are present in Ni electrocatalysts.[26,29–31] This trend is,

however, not observed in Figure 3 for increasing electrolytic Fe concentrations.

The CV results (Figure 3), therefore, indicate that Fe is not incorporated into the bulk structure of the Ni electrocatalysts since Fe incorporation into the bulk would have resulted in an anodic shift and decreased intensity of the oxidation peak as the Fe concentration increases.[29] The CVs in this study do not exhibit these changes and this can be attributed to the fact that Fe did not incorporate into the bulk electrocatalyst structures. In addition, the broad redox peaks and the occasional presence of a second oxidation and/or reduction peak could indicate that Fe is not homogeneously distributed throughout the electrocatalysts in this study.

Linear sweep voltammetry was performed to obtain information about the OER activity of the different electrocatalysts in different Fe concentrations (**Figure 4**). In order for a clearer comparison between the samples, an estimate of the electrochemically active surface area (ECSA) of each electrocatalyst
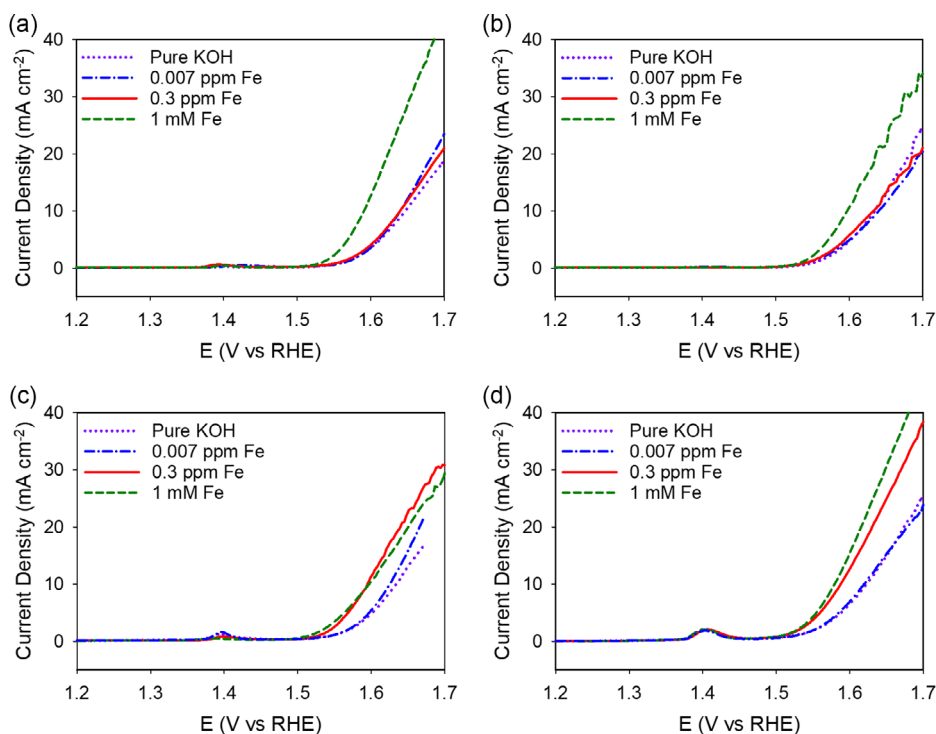
Figure 4. LSVs of a) colloidal Ni, b) colloidal NiO, c) NiO nanoparticles, and d) NiNiO nanoparticles after 30 CV cycles in pure KOH, and KOH containing 0.007, 0.3 ppm, and 1 mM Fe.

sample in each electrolyte composition has been determined in terms of the double layer capacitance, using cyclic voltammetry, and can be seen in Section 6 of the supporting information. It can be seen that the addition of Fe in the electrolyte has only a small effect on the ECSA of these electrodes, and, therefore, the effect of different Fe concentrations on the activity of the electrocatalysts cannot be explained by ECSA alone. A widely accepted benchmark for the activity of OER electrocatalysts is the value of the overpotential at 10 mA cm^{-2}. Therefore, this benchmark is
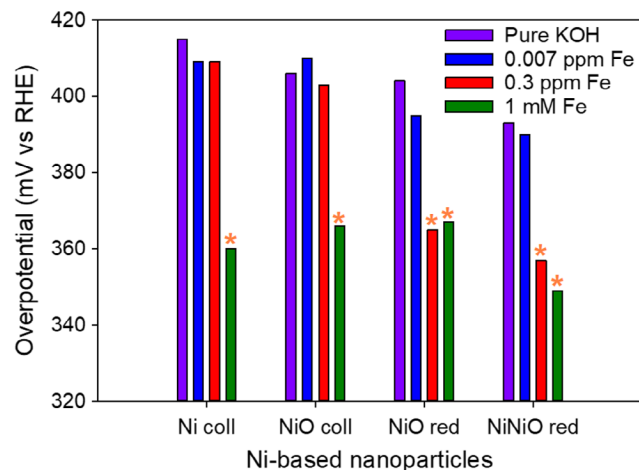

Figure 5. A bar chart summarizing the OER overpotentials at 10 mA cm^{-2} of each of the Ni-based electrocatalysts after 30 CV cycles in pure KOH (purple), 0.007 ppm Fe (green), 0.3 ppm Fe (red), and 1 mM Fe (green).

also used in this study to evaluate and compare the OER activities of different Ni-based electrocatalysts in KOH containing different concentrations of Fe. In this regard, Ni nanoparticles were not included, as the current density did not reach the targeted 10 mA cm^{-2} below 1.7 V. The bar chart in **Figure 5** concisely summarizes the overpotential at 10 mA cm^{-2} for each of the electrocatalysts after 30 CV cycles in pure KOH and KOH containing 0.3 ppm Fe and 1 mM Fe. The orange stars in the figure indicate which samples had peaks corresponding to FeOOH in their in situ Raman spectra and will be subsequently discussed.

Colloidal Ni and NiO exhibit a significant decrease in overpotential when the samples are cycled in KOH containing 1 mM Fe. The overpotential decreases with 55 mV for colloidal Ni and 40 mV for colloidal NiO when 1 mM Fe is added to 0.1 M KOH. Second, the OER activities of the nanoparticles prepared by chemical reduction significantly decrease after the addition of only 0.3 ppm Fe. The overpotential of NiO nanoparticles at 10 mA cm^{-2} decreases with 39 mV when 0.3 ppm Fe is present in the electrolyte, and that of NiNiO with 36 mV. The overpotentials (at 10 mA cm^{-2}) of the samples cycled in pure KOH and 0.007 ppm Fe are in good agreement with that of Ni samples in pure KOH with no effect of Fe.[15] The overpotential of samples cycled in 1 mM Fe agrees well with Ni electrocatalysts tested in reagent grade KOH (containing Fe impurities),[32] NiFe electrocatalysts[17] and that of Ni samples that have incorporated Fe.[15] The results of this study are also in good agreement with that reported by Corrigan, indicating that an Fe concentration of 1 ppm Fe significantly enhances the OER activity of Ni electrocatalysts.[11] In addition, it is

clear that 0.3 ppm Fe dramatically increases the OER activity of the nanoparticles prepared by the chemical reduction method. Since reagent-grade KOH in pellet form is reported to contain ≤ 0.66 ppm Fe, these results show that studies reporting Ni activities in reagent-grade KOH will have to be repeated in pure KOH to get a true indication of the iron-free OER activity of Ni.

The as-prepared nanoparticles could possibly have contained trace amounts of Fe. This Fe could have originated from the Ni precursors used to prepare the electrocatalysts or the different reagents used in the nanoparticle preparation as well as ink preparation. This could be the reason why no significant increase in OER activity is observed for the nanoparticle OER electrocatalysts when Fe concentrations under 0.3 ppm are present in the electrolyte. In other words, this accounts for the similar overpotentials observed for the samples cycled in pure KOH and 0.007 ppm Fe. The slightly lower overpotential for the colloidal NiO sample cycled in pure KOH compared to the sample cycled in 0.007 ppm Fe is simply ascribed to the margin of error of linear sweep voltammogram (LSV) experiments, and we thus consider that the activities are essentially the same.

Figure 5 also shows that each unique synthesis method leads to a unique Fe saturation concentration for the electrocatalysts. This is the point where increasing the electrolytic Fe concentration further has no influence on the OER activity. This concentration is the lowest for Ni samples prepared by chemical reduction (0.3 ppm) and the highest for colloidal nanoparticles (1 mM). The morphologies of the electrocatalysts might explain the different saturation points. The morphology of the particles prepared by chemical reduction (Figure 1) likely has more defect and edge sites for Fe to adsorb, leading to saturation at a lower concentration.

Lastly, it should be noted that the oxidation states of the electrocatalysts do not have a significant effect on the electrocatalytic activity. The overpotentials of all the nanoparticles after cycling in pure KOH are between 393 and 415 mV at 10 mA cm^{-2}. After cycling in 1 mM Fe, their overpotentials are between 349 and 367 mV at 10 mA cm^{-2}. The Ni and NiO samples exhibit very similar overpotentials despite their different oxidation states. The XPS investigation (Section 4 in the supporting information) indicates that Ni and NiO have varying oxidation states after being tested in the alkaline electrolyte. The NiNiO sample exhibits the lowest overpotential, though not significantly lower than the other samples. Only one oxidation state was observed in the XPS spectra for this sample after electrochemical testing, while all other samples exhibited two different oxidation states (Section 4, Supporting Information).

2.2. In Situ Raman Spectroscopy

In the Raman spectra, the characteristic doublet at 480 and 560 cm^{-1} (**Figure 6** and **7**) correspond to the most prominent peaks of NiOOH. The peak at 560 cm^{-1} arises due to the O–Ni–O stretching (polarized A_{1g}) mode and the peak at 480 cm^{-1} represents the O–Ni–O bending (depolarized E_g) mode of NiOOH.[16,33] A broad peak centered around 500 cm^{-1} can also be observed in these figures. This peak may be ascribed to the Ni–O stretching vibration of NiO or Ni(OH)$_2$. This species arises

upon contact with air or alkaline electrolyte, where a surface layer of Ni is oxidized to NiO[27] or Ni(OH)$_2$,[9,14] respectively.

Previous studies state that Fe from the electrolyte will incorporate into the bulk of Ni electrocatalysts to form a NiFe-LDH structure.[24] When Fe is incorporated into Ni electrocatalysts, it replaces some of the lattice Ni in NiOOH, resulting in an NiFe LDH structure. This structure can be identified in Raman spectra by examining the two peaks at $\approx$480 and 560 cm^{-1}, ascribed to the Ni–O vibrations of NiOOH.[24,34,35] When an NiFe LDH structure is present, the 560 cm^{-1} peak increases in intensity relative to the 480 cm^{-1} peak and these peaks appear noticeably broader.[24] In addition, no peaks corresponding to a separate Fe phase are present when Fe is present in the bulk of Ni electrocatalysts.

Various factors influence Fe incorporation into the bulk. This includes the time that the Ni electrocatalyst is in contact with the electrolyte and the concentration of this electrolyte. Fe incorporation is said to be diffusion limited and therefore depends on the amount of time that the electrode is in contact with the Fe-containing electrolyte.[26] It is also not clear whether applied potential or potential cycling is necessary for Fe incorporation. Fe first adsorbs to the Ni electrocatalyst surface (specifically at edge or defect sites) and enhances the OER activity before incorporating into the bulk over time.[29] A study that reports the presence of a NiFe LDH structure aged a Ni electrode in Fe-containing KOH for a minimum period of 24 h.[24] This is 23 h and 30 min more than the electrodes in this study are in contact with Fe-containing electrolyte. Thus, the surface Fe observed in this study has possibly not had enough time to incorporate into the bulk structure to replace some of the Ni.

Figure 6 and 7 show the Raman spectra of Ni electrocatalysts at 1.42 V vs reversible hydrogen electrode (RHE) before and after cycling in pure KOH and KOH containing different concentrations of Fe, respectively. Furthermore, **Table 1** summarizes the peak positions and 480/560 cm^{-1} peak height ratios of the peaks in these Raman spectra.

There are two main findings in the Raman spectra for Ni nanoparticles that serve as evidence that Fe is present on the surface of Ni catalysts and not in bulk. First, from the Raman investigation, it is evident that the 480/560 cm^{-1} peak height ratio does not decrease with increasing Fe concentration (see also Table 1). In addition, the peaks do not appear broader after Fe addition. This means that the presence of a NiFe-LDH structure is not detected.

Furthermore, Table 1 shows that there is inconsistency in the 480/560 cm^{-1} peak height ratios. This is in accordance with a recent study that reported in situ Raman spectra of a FeOOH–NiOOH electrocatalyst (a NiOOH electrocatalyst with FeOOH covalently bonded to the surface).[36] This study reported that surface FeOOH results in a heterogeneous structure and that three points on the same electrocatalyst surface could yield Raman spectra with varying peak positions and intensities.[36] This is because the FeOOH occurs as clusters that are covalently bonded to the surface.[36]

What is also important to note is that the 480/560 cm^{-1} peak height ratio for NiFe LDH is reported as 1.18, where that of FeOOH-NiOOH is 1.78 and that of NiOOH is 2.2 (importantly, all of these values refer to peak height ratios measured at 0.6 V vs.
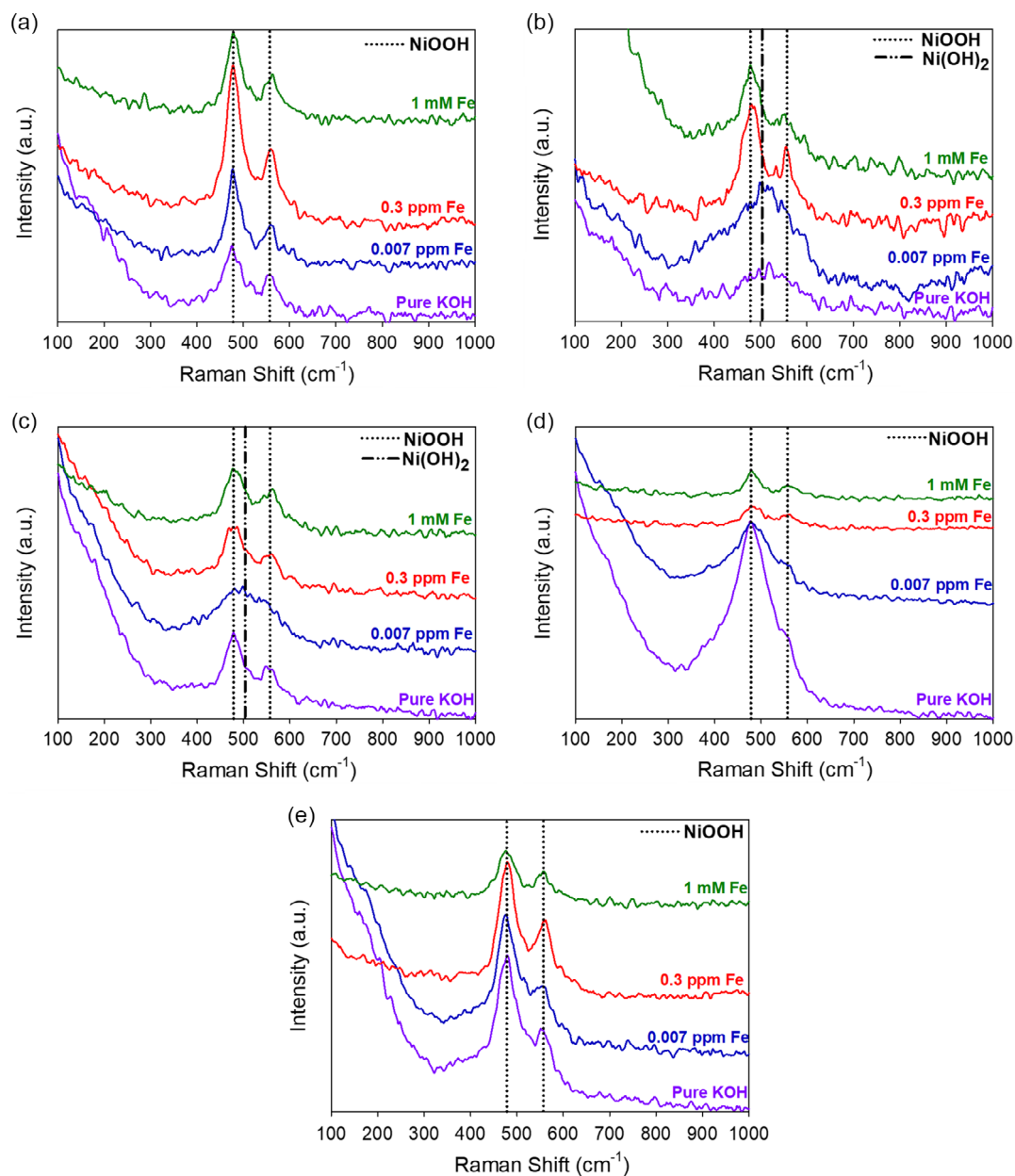
Figure 6. In situ Raman spectra of a) colloidal Ni, b) colloidal NiO, c) Ni nanoparticles, d) NiO nanoparticles, and e) NiNiO nanoparticles, in pure KOH and KOH, doped with 0.007, 0.3 ppm, and 1 mM Fe.

Hg/HgO).[36] Table 1 indicates that the peak height ratios at 0.6 V vs Hg/HgO of the electrocatalysts in this study are between 1.5 and 2. This is a further indication that the samples in this study are either Ni (in various oxidation states) or FeOOH surface-bound to Ni electrocatalysts and not NiFe LDH.

The second important observation from the Raman spectra is that peaks corresponding to α–FeOOH (these peaks appear at around 303, 400, and 675 cm^{-1}, and are the three most prominent peaks in the Raman spectrum of α–FeOOH[37,38]) are present for colloidal Ni and NiO cycled in KOH containing 1 mM Fe. These Fe peaks are also present in the spectra of NiO and NiNiO nanoparticles cycled in 0.3 ppm Fe and 1 mM Fe. Furthermore,

the NiNiO sample cycled in 0.3 ppm Fe has peaks at 986 and 1062 cm^{-1}. There is a possibility that these peaks arise due to Nafion.[39] However, α–FeOOH also has clear peaks at similar wavenumbers.[40] Based on the clear evidence that α–FeOOH is present with increased OER activity, these peaks will be assumed to arise due to its presence. What is also of interest is that α–FeOOH is present and not γ–FeOOH, as reported in a similar study of surface Fe.[36] α–FeOOH is crystalline and thermodynamically more stable than amorphous γ–FeOOH.[40]

These peaks corresponding to α–FeOOH are illustrated by the orange stars in Figure 5. The presence of these peaks is directly
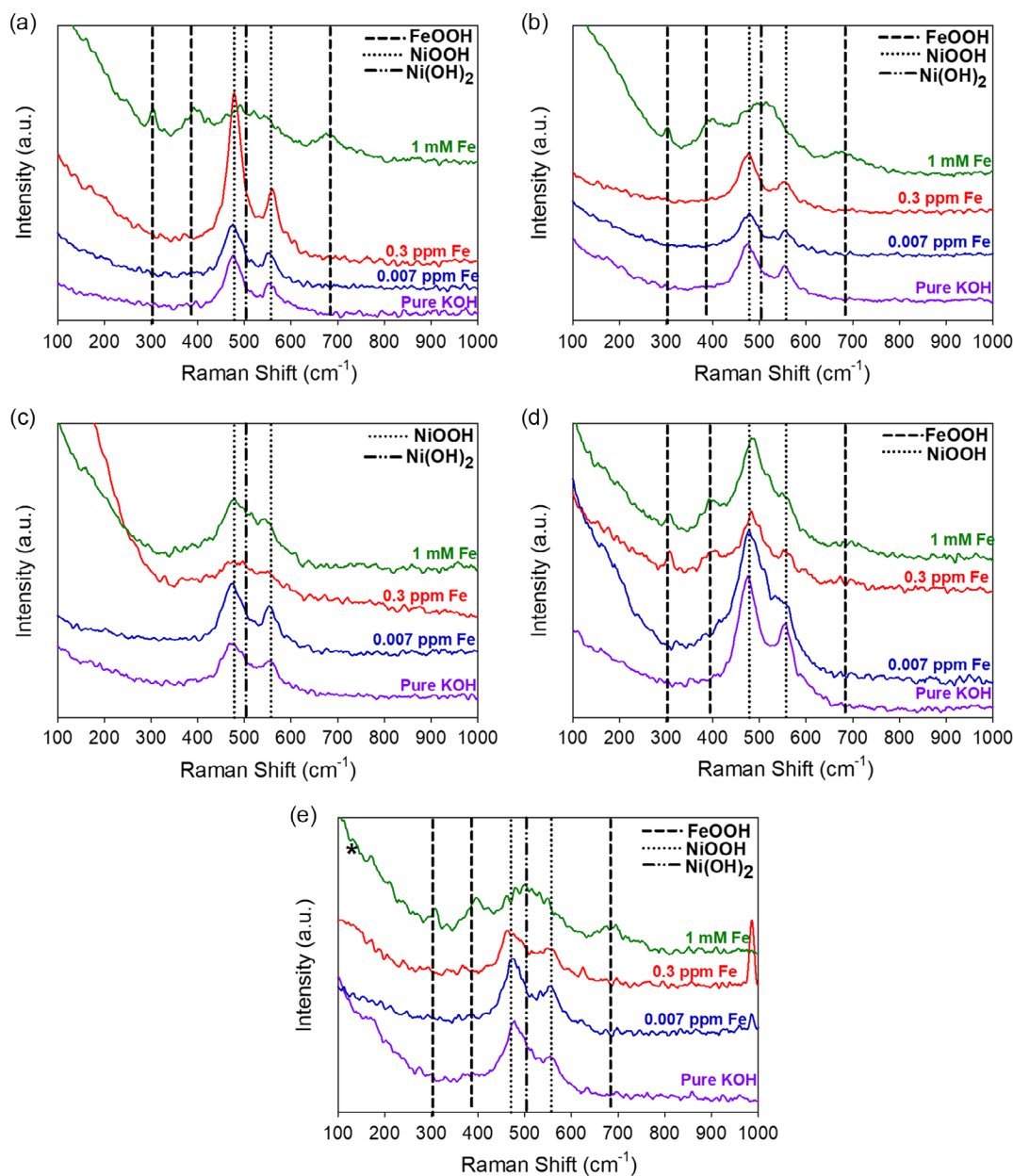
Figure 7. In situ Raman spectra of a) colloidal Ni, b) colloidal NiO, c) Ni nanoparticles, d) NiO nanoparticles, and e) NiNiO nanoparticles, after 30 CV cycles in pure KOH and KOH doped with 0.007, 0.3 ppm and 1 mM Fe. *The peaks at 1.27 V are shown for this sample as they appear clearer than at 1.42 V.

Table 1. The 480/560 cm^{-1} peak height ratios of Ni, NiO, and NiNiO nanoparticle electrocatalysts at 1.42 V in pure KOH and KOH doped with 0.007 0.3 ppm, and 1 mM Fe.

	Pure KOH	0.007 ppm Fe	0.3 ppm Fe	1 mM Fe
Colloidal Ni	2.0	2.0	2.9	–
Colloidal NiO	1.7	2.0	2.0	–
Ni nanoparticles	1.5	1.4	–	–
NiO nanoparticles	1.6	1.6	2.0	–
NiNiO nanoparticles	1.5	1.6	–	–

correlated to a decrease in OER overpotential. In addition, the overpotentials of Ni nanoparticles prepared by the reduction method do not decrease upon the addition of any amount of Fe to the electrolyte. Accordingly, no α–FeOOH peaks are observed in the in situ Raman spectra for this electrocatalyst.

It is unlikely that the Fe peaks detected through Raman spectroscopy originate from the Fe in the electrolyte and not the Fe bound to the surface of the electrocatalyst. The Raman spectra of the samples before they were cycled contain no Fe peaks, regardless of the presence of electrolytic Fe during the Raman measurement. If the α–FeOOH peaks originated from

the Fe in the electrolyte, they would have been visible in the spectra of the uncycled samples as well. However, the α–FeOOH peaks are only visible after cycling, indicating that Fe adsorbs to the surface of Ni electrocatalysts during the potential cycling process.

3. Conclusion

The performance of Ni, NiNiO, and NiO electrocatalysts for the OER is linked to the presence of a separate α–FeOOH phase as detected by in situ Raman spectroscopy; α–FeOOH peaks were seen in the Raman spectra in all instances in which a significant decrease in the OER overpotential was also observed. In addition, the ratio of the height of the 480 cm^{-1} peak to that of the 560 cm^{-1} peak in the Raman spectra did not decrease with increasing Fe concentration in the electrolyte, even though the electrocatalytic activity did increase. This indicates that the enhanced activity observed when iron is incorporated in Ni and NiO electrocatalysts is related to iron in the catalyst surface rather than Fe incorporated in the bulk of the electrocatalyst. This information is important toward identifying the role of Fe in enhancing the electrochemical activity of these electrocatalysts. A more in depth understanding of how the α–FeOOH enhances the OER activity is still needed. This will be crucial toward the development of better-performing electrocatalysts for the sluggish anodic OER in alkaline media.

4. Experimental Section

Electrocatalyst Preparation: Two different synthesis methods were followed in this study to synthesize nanoparticles with two different morphologies. The first synthesis method was based on a tailored method to produce monodispersed, colloidal nanoparticles using oleylamine (OAm) as the reducing agent and tri-*n*-octylphosphine (TOP) as a surface stabilizer.[4] The second synthesis method was based on the chemical reduction of nickel(II) nitrate hexahydrate with sodium borohydride as reducing agent and produced nanoparticles.[6,7]

To produce colloidal nanoparticles, 50 mL of oleylamine (OAm; technical grade, 70%, Sigma Aldrich), 4 g of nickel(II) acetylacetonate (Ni(acac)$_2$; anhydrous, 95%, Sigma Aldrich) and 14 mL of tri-*n*-octylphosphine (TOP, 97%, Sigma Aldrich) were heated for 5 min at 50 °C and then for 2 h in an inert environment at 220 °C while stirring. To clean these nanoparticles, toluene (anhydrous, 99.8%, Sigma Aldrich) and isopropanol (IPA, 99.5%, Sigma Aldrich) were used during centrifugation. After the supernatant was decanted, the particles were dried in a vacuum oven for 22 h at 60 °C. For Ni, the particles were used as-prepared. NiO was formed by annealing a portion of the Ni particles in a tube furnace for 4 h at 600 °C.

To prepare nanoparticles employing the chemical reduction method, 2.911 g of nickel(II) nitrate hexahydrate (Ni(NO$_3$)$_2$·6H$_2$O; ≥97.0%, Sigma Aldrich) was added to 100 mL deionized (DI) water (18.2 MΩ cm^{-1}, 3 ppb TOC, Milli-*Q* water) and stirred for 10 min. 1.895 g of NaBH$_4$ (98%, Sigma Aldrich) was added to 500 mL water, and then the Ni(NO$_3$)$_2$·6H$_2$O solution was quickly added and stirred for 30 min. The mixture was centrifuged to obtain the particles. The particles were subsequently cleaned by centrifuging with water and ethanol. The washed particles were dried in a vacuum oven at 60 °C for 20 h. The particles were annealed at 500 °C for 6 h in air to yield NiO, and in 5% H$_2$/Ar at 500 °C to yield Ni. To form NiNiO, the particles were annealed in air and subsequently in 5% H$_2$/Ar.

The nanoparticles from both syntheses each require a unique ink recipe to ensure optimum dispersion. Both inks contain DI water, isopropanol (Sigma Aldrich), and 0.05 mL (5 wt%) Nafion 117 solution (Sigma

Aldrich). For the particles prepared via the chemical reduction method, an ink was formulated for these particles containing 0.85 mL IPA and 0.15 mL water together with 0.05 mL Nafion and 10 mg particles. The ink prepared for the tailored particles consists of 0.75 mL water, 0.25 mL IPA, 0.05 mL Nafion, and 10 mg electrocatalyst powder. Both inks were ultrasonicated for 15 min to provide a homogeneous dispersion before drop-casting.

Physical Characterization: Transmission electron microscopy (TEM) analysis was performed with a Jeol JEM 2100-LaB6 microscope. The TEM images of the colloidal particles in this study were analyzed with ImageJ software. Powder X-ray diffraction analysis (XRD) patterns were obtained for each of the synthesized particles using a Bruker D8 A25 DaVinci X-ray Diffractometer with Cu-K$_\alpha$ radiation and a LynxEye superspeed detector. For the nanoparticles, spectra were obtained in the 2θ-range 15°–75° with a step size of 0.02° (2θ). For colloidal nanoparticles, spectra were obtained in the 2θ-range 20°–80°. The 2θ ranges were selected according to what was previously reported in the literature for each morphology to successfully characterize them.[4,7]

Electrochemistry: Rotating disk glassy carbon (GC) electrodes (5 mm diameter, Pine Research) were polished using 0.3 and 0.05 μm alumina (Al$_2$O$_3$) suspensions (Allied High-Tech Products, Inc.) on microfiber polishing pads. The electrodes were rinsed with DI water between polishing with different particle sizes. After polishing, the GC electrodes were sonicated in DI water for 50 s and then in 1 M purified KOH for 60 s to dissolve any alumina particles left on the surface.

Four electrolytes were used in this study: pure 0.1 M KOH and 0.1 M KOH doped with 0.007, 0.3 ppm, and 1 mM of Fe. To make a pure 0.1 M KOH solution, 0.561 g semiconductor grade KOH pellets (99.99%, Sigma Aldrich) were weighed and made up to a 1 L solution by adding DI water (18.2 MΩ cm^{-1}, 3 ppb TOC, Milli-Q water). To avoid Fe contamination, no glass components were used in this process, and KOH solutions were stored in plastic containers. Iron(III) nitrate nonahydrate (Fe(NO$_3$)$_3$·9H$_2$O, 99.9999% trace metals basis, Sigma Aldrich) was added to 0.1 M KOH to obtain 0.007, 0.3 ppm, and 1 mM Fe.

A standard three-electrode electrochemical cell was used to perform all the electrochemical analysis techniques in this study. A Teflon cell was used and was thoroughly cleaned before use and in between experiments to eliminate Fe-contamination. For cleaning, the Teflon cell was soaked in 1 M sulfuric acid (H$_2$SO$_4$) for 3 h and boiled in DI water three times, replacing the water each time.

A Pt wire was used as the counter electrode (CE), and an Hg/HgO (Pine research) reference electrode (RE) was employed. The GC working electrode (WE) was used as part of an rotating disk electrode (RDE) setup (Pine Research). Pt CEs were periodically cleaned by submerging in 1 M sulfuric acid for 1 min. The electrodes were connected to a Bio-Logic (VMP3) potentiostat controlled with EC-Lab software. The electrolyte was saturated with Ar, and all experiments were performed at room temperature. An inert gas was chosen to eliminate any effect that oxygen might have on the redox features since the examination of the redox features is an important part of this study. It has been shown in a previous publication that removing dissolved oxygen does not have an effect on the OER activity.[41]

The Hg/HgO RE was calibrated by performing a CV at a scan rate of 10 mV s^{-1} between −1.0 and 0.9 V in H$_2$ saturated 0.1 M KOH with a Pt WE and CE. The average value of the voltage intercept of the forward and backward scans was 0.87 V. Therefore, 0.87 V is the offset potential used to convert measured potentials to the RHE scale. The equilibrium potential is 1.29 V vs RHE, which was subtracted from the measured potential to obtain the overpotential. The Ohmic (IR) drop was corrected by using the ohmic drop correction (ZIR) function of EC-Lab software. An electrochemical impedance spectroscopy measurement was performed prior to each experiment to provide an estimate of the ohmic resistance. The frequency range used was 0.1–10^5 Hz and alternative current (AC) perturbation amplitude of 10 mV. The real part of the impedance at high frequency was taken as the ohmic resistance. The compensation level was 85% of the measured ohmic resistance, and the IR drop was compensated in situ by the potentiostat software.

In this study, the current density is reported by using the geometric surface area of the WE. It is worth taking note of the mass loading of these

electrodes as well. Since 10 µL of ink is drop-casted on each GC electrode, the mass loading of the electrocatalysts is 0.095 mg on a GC electrode with a surface area of 0.196 cm^{-2}. The mass loading is, therefore, 0.485 mg cm^{-2}.

CVs of each electrocatalyst were recorded in pure KOH and Fe-containing KOH (0.007, 0.3 ppm, and 1 mM Fe). These three concentrations were chosen based on values reported in similar studies.[15,24,26,29] 0.007 ppm Fe is in the range of the amount of Fe expected in TraceSELECT or otherwise pure commercially available KOH (99–99.9%),[15] and 0.3 ppm is in the range of the amount of Fe expected in reagent grade KOH.[24] CV experiments were performed between 1 and 1.67 V vs RHE at a scan rate of 20 mV s^{-1} while the WE was rotated at 1600 rpm. This potential range was chosen as it allows for preconditioning but at the same time shows the OER activity of the electrocatalysts. LSV experiments were performed between 1 and 1.67 V vs RHE at a scan rate of 1 mV s^{-1}, while the WE was rotated at 1600 rpm. Such a slow scan rate was employed to resemble steady-state conditions. LSV was performed for each electrocatalyst in each electrolyte after 30 CV cycles were completed.

In Situ Raman Spectroscopy: In situ Raman spectra were recorded employing a confocal Raman microscope (WITec alpha300 R) with 5 mW of power delivered by a laser operating at 532 nm. A Zeiss EC Epiplan objective (10×magnification) was used. The instrument was controlled with WITec control scanning and data acquisition software. Prior to each experiment, the calibration of the instrument was confirmed against a Si wafer.

A Teflon-sheathed WE disk was mounted within a custom-made Teflon cell facing upwards toward the Raman microscope. A Pt CE and an Hg/HgO RE were used for the electrochemical measurements. The working, counter, and REs were connected to a (Ivium-n-Stat) potentiostat, which controlled the potential applied to the WE in chronoamperometry experiments (potential steps). An image of the in situ setup can be seen in Figure S1, Supporting Information.

Two sets of samples were investigated: as-prepared samples and samples that were subjected to 30 potential cycles (CVs) prior to the Raman analysis. The following potential steps were applied to the as-prepared electrodes from open circuit potential (OCP): 1.27, 1.37, 1.42, and 1.47 V vs RHE. Each potential step was held for 1000 s to obtain a Raman spectrum at a stabilized current. After 30 activation CVs, the WE was subjected to the following potentials, stepped from OCP: 1.17, 1.27, 1.37, 1.42, and 1.47 V vs RHE. It was found that 500 s at each potential was sufficient to obtain a stable current. The potential was allowed more time to stabilize for the electrocatalysts that have not been subjected to the activation CVs yet (the as-prepared samples), as these surfaces were less stable. The potential should not be increased above 1.47 V vs RHE as this results in excessive bubble formation due to the OER, which would obscure Raman measurements.

Supporting Information

Supporting Information is available from the Wiley Online Library or from the author.

Conflict of Interest

The authors declare no conflict of interest.

Data Availability Statement

The data that support the findings of this study are available from the corresponding author upon reasonable request.

[1] C. G. Fink, *Ind. Eng. Chem.* **1924**, *16*, 566.
[2] V. Vij, S. Sultan, A. M. Harzandi, A. Meena, J. N. Tiwari, W.-G. Lee, T. Yoon, K. S. Kim, *ACS Catal.* **2017**, *7*, 7196.
[3] Y. Chen, K. Rui, J. Zhu, S. X. Dou, W. Sun, *Chem. Eur. J.* **2019**, *25*, 703.
[4] S. Carenco, C. Boissière, L. Nicole, C. Sanchez, P. Le Floch, N. Mézailles, *Chem. Mater.* **2010**, *22*, 1340.
[5] S. Carenco, *Chem. Rec.* **2018**, *18*, 1114.
[6] M. K. Bates, Q. Jia, N. Ramaswamy, R. J. Allen, S. Mukerjee, *J. Phys. Chem. C* **2015**, *119*, 5467.
[7] A. Y. Faid, A. O. Barnett, F. Seland, S. Sunde, *Electrochim. Acta* **2020**, *361*, 137040.
[8] I. M. Sadiek, A. M. Mohammad, M. E. El-Shakre, M. S. El-Deab, *Int. J. Hydrogen Energy* **2012**, *37*, 68.
[9] F. Chekin, H. Tahermansouri, M. R. Besharat, *J. Solid State Electrochem.* **2014**, *18*, 747.
[10] M. Tahir, L. Pan, F. Idrees, X. Zhang, L. Wang, J.-J. Zou, Z. L. Wang, *Nano Energy* **2017**, *37*, 136.
[11] D. A. Corrigan, *J. Electrochem. Soc.* **1987**, *134*, 377.
[12] M. Gao, W. Sheng, Z. Zhuang, Q. Fang, S. Gu, J. Jiang, Y. Yan, *J. Am. Chem. Soc.* **2014**, *136*, 7077.
[13] P. Ganesan, A. Sivanantham, S. Shanmugam, *J. Mater. Chem. A* **2016**, *4*, 16394.
[14] K. Fominykh, J. M. Feckl, J. Sicklinger, M. Döblinger, S. Böcklein, J. Ziegler, L. Peter, J. Rathousky, E. Scheidt, T. Bein, *Adv. Funct. Mater.* **2014**, *24*, 3123.
[15] L. Trotochaud, S. L. Young, J. K. Ranney, S. W. Boettcher, *J. Am. Chem. Soc.* **2014**, *136*, 6744.
[16] S. Lee, L. Bai, X. Hu, *Angew. Chem. Int. Ed.* **2020**, *59*, 8072.
[17] C. Peng, N. Ran, G. Wan, W. Zhao, Z. Kuang, Z. Lu, C. Sun, J. Liu, L. Wang, H. Chen, *ChemSusChem* **2020**, *13*, 811.
[18] Z. Yang, X. Liang, *Nano Res.* **2020**, *13*, 461.
[19] J. Li, R. Lian, J. Wang, S. He, Z. Rui, *Electrochim. Acta* **2020**, *331*, 135395.

[20] R. Wang, C. Wang, S. Yin, Y. Peng, J. Chen, Y. Deng, J. Li, *Catal. Today* **2020**, *364*, 140.

[21] K. Zhu, X. Zhu, W. Yang, *Angew. Chem. Int. Ed.* **2019**, *58*, 1252.

[22] M. Chen, D. Liu, L. Qiao, P. Zhou, J. Feng, K. W. Ng, Q. Liu, S. Wang, H. Pan, *Chem. Eng. J.* **2023**, *461*, 141939.

[23] Y. AlSalka, S. Schwabe, J. Geweke, G. Ctistis, H. Wackerbarth, *Energy Technol.* **2023**, *11*, 2200788.

[24] S. Klaus, Y. Cai, M. W. Louie, L. Trotochaud, A. T. Bell, *J. Phys. Chem. C* **2015**, *119*, 7243.

[25] L. A. García-Cerda, K. M. Bernal-Ramos, S. M. Montemayor, M. A. Quevedo-López, R. Betancourt-Galindo, D. Bueno-Báques, *J. Nanomater.* **2011**, *2011*, 162495.

[26] K. L. Nardi, N. Yang, C. F. Dickens, A. L. Strickler, S. F. Bent, *Adv. Energy Mater.* **2015**, *5*, 1500412.

[27] M. E. G. Lyons, M. P. Brandon, *Int. J. Electrochem. Sci* **2008**, *3*, 1386.

[28] R. L. Doyle, I. J. Godwin, M. P. Brandon, M. E. G. Lyons, *Phys. Chem. Chem. Phys.* **2013**, *15*, 13737.

[29] M. Burke Stevens, C. D. M. Trang, L. J. Enman, J. Deng, S. W. Boettcher, *J. Am. Chem. Soc.* **2017**, *139*, 11361.

[30] D. Friebel, M. W. Louie, M. Bajdich, K. E. Sanwald, Y. Cai, A. M. Wise, M.-J. Cheng, D. Sokaras, T.-C. Weng, R. Alonso-Mori, *J. Am. Chem. Soc.* **2015**, *137*, 1305.

[31] M. W. Louie, A. T. Bell, *J. Am. Chem. Soc.* **2013**, *135*, 12329.

[32] L.-A. Stern, X. Hu, *Faraday Discuss.* **2015**, *176*, 363.

[33] J. D. Michael, E. L. Demeter, S. M. Illes, Q. Fan, J. R. Boes, J. R. Kitchin, *J. Phys. Chem. C* **2015**, *119*, 11475.

[34] B. Siang Yeo, A. T. Bell, *J. Phys. Chem. C* **2012**, *116*, 8394.

[35] R. Kostecki, F. McLarnon, *J. Electrochem. Soc.* **1997**, *144*, 485.

[36] L. Bai, S. Lee, X. Hu, *Angew. Chem.* **2020**, *133*, 3132.

[37] M. V. Abrashev, V. G. Ivanov, B. S. Stefanov, N. D. Todorov, J. Rosell, V. Skumryev, *J. Appl. Phys.* **2020**, *127*, 205108.

[38] K. Hedenstedt, J. Bäckström, E. Ahlberg, *J. Electrochem. Soc.* **2017**, *164*, H621.

[39] S. Logette, C. Eysseric, P. Huguet, C. Gavach, G. Pourcelly, *J. Appl. Electrochem.* **1999**, *29*, 371.

[40] W. Luo, C. Jiang, Y. Li, S. A. Shevlin, X. Han, K. Qiu, Y. Cheng, Z. Guo, W. Huang, J. Tang, *J. Mater. Chem. A* **2017**, *5*, 2021.

[41] A. C. Garcia, M. T. M. Koper, *ACS Catal.* **2018**, *8*, 9359.